

Operando Study of Thermal Oxidation of Monolayer MoS₂

Sangwook Park, Angel T. Garcia-Esparza, Hadi Abroshan, Baxter Abraham, John Vinson, Alessandro Gallo, Dennis Nordlund, Joonsuk Park, Taeho Roy Kim, Lauren Vallez, Roberto Alonso-Mori, Dimosthenis Sokaras,* and Xiaolin Zheng*

Monolayer MoS₂ is a promising semiconductor to overcome the physical dimension limits of microelectronic devices. Understanding the thermochemical stability of MoS₂ is essential since these devices generate heat and are susceptible to oxidative environments. Herein, the promoting effect of molybdenum oxides (MoO_x) particles on the thermal oxidation of MoS₂ monolayers is shown by employing operando X-ray absorption spectroscopy, ex situ scanning electron microscopy and X-ray photoelectron spectroscopy. The study demonstrates that chemical vapor deposition-grown MoS₂ monolayers contain intrinsic MoO_x and are quickly oxidized at 100 °C (3 vol% O₂/He), in contrast to previously reported oxidation thresholds (e.g., 250 °C, $t \leq 1$ h in the air). Otherwise, removing MoO_x increases the thermal oxidation onset temperature of monolayer MoS₂ to 300 °C. These results indicate that MoO_x promote oxidation. An oxide-free lattice is critical to the long-term stability of monolayer MoS₂ in state-of-the-art 2D electronic, optical, and catalytic applications.

Towards these visions, great progress has been made on the synthesis of wafer-scale polycrystalline MoS₂ monolayers,^[7] and large-domain (≈ 500 μm) single-crystalline MoS₂ monolayers by chemical vapor deposition (CVD),^[2] and the wafer-scale transfer and stacking of monolayer MoS₂ for heterogeneous integrations.^[8,9] In practice, microelectronics dissipate energy through Joule heating,^[10] and MoS₂ monolayer transistors reach average operating temperatures of >150 °C with local hot spots of >250 °C.^[10,11] Therefore, investigating the thermochemical stability of MoS₂ above room temperature (RT) and under the device working temperature range is important.

Past studies on the thermal oxidation of MoS₂ reported that the oxidation process is fast when the temperature is above ≈ 250 °C (e.g., 250 °C in the air for 1 h,^[12]


Monolayer molybdenum disulfide (MoS₂) is an atomically thin semiconductor with a sub-nanometer thickness (6.5–8 Å),^[1,2] high electron mobility (≈ 200 cm² V⁻¹ s⁻¹),^[1] a direct band gap (1.8–2.2 eV),^[1,3] and high current on/off ratio ($>10^8$).^[1] MoS₂ monolayers^[4] can potentially be used for flexible electronics and push the physical dimension limits of microelectronics.^[4–6]

360 °C in the air for 5 min,^[13] and 380 °C in the air for 10 min; Table S1, Supporting Information).^[10] These findings were supported by ex situ observations of pits and crack formation, and identification of molybdenum oxides via atomic force microscopy (AFM),^[12–16] scanning electron microscopy (SEM),^[13,15,17] transmission electron microscopy (TEM),^[17] X-ray photoelectron

Dr. S. Park, Dr. A. T. Garcia-Esparza, L. Vallez, Prof. X. Zheng
Department of Mechanical Engineering
Stanford University
Stanford, CA 94305, USA
E-mail: xlzheng@stanford.edu

Dr. S. Park
Department of Mechanical Engineering
Seoul National University
Seoul 08826, South Korea

Dr. A. T. Garcia-Esparza, Dr. B. Abraham, Dr. D. Nordlund, Dr. D. Sokaras
Stanford Synchrotron Radiation Lightsource
SLAC National Accelerator Laboratory
2575 Sand Hill Road Menlo Park, CA 94025, USA
E-mail: dsokaras@slac.stanford.edu

 The ORCID identification number(s) for the author(s) of this article can be found under <https://doi.org/10.1002/advs.202002768>

© 2021 The Authors. Advanced Science published by Wiley-VCH GmbH. This is an open access article under the terms of the Creative Commons Attribution License, which permits use, distribution and reproduction in any medium, provided the original work is properly cited.

DOI: 10.1002/advs.202002768

Dr. H. Abroshan, Dr. A. Gallo
SUNCAT Center for Interface Science and Catalysis
SLAC National Accelerator Laboratory
2575 Sand Hill Road Menlo Park, CA 94025, USA

Dr. H. Abroshan
School of Chemistry and Biochemistry
Georgia Institute of Technology
Atlanta GA 30332, USA

Dr. B. Abraham, Dr. R. Alonso-Mori
Linac Coherent Light Source
SLAC National Accelerator Laboratory
2575 Sand Hill Road Menlo Park, CA 94025, USA

Dr. J. Vinson
National Institute of Standards and Technology
100 Bureau Drive Gaithersburg, MD 20899, USA

Dr. J. Park
Materials Science and Engineering
Stanford University
Stanford CA 94305, USA

Dr. T. R. Kim
Stanford Nano Shared Facilities
Stanford University
Stanford CA 94305, USA

spectroscopy (XPS),^[12,16,17] nanomechanical means,^[16] and Raman spectroscopy.^[14] Such ex situ characterization methods, although very informative, may not detect subtle morphological and chemical compositional changes brought on by MoS₂ oxidation. Importantly, the previous thermal oxidation studies assumed chemically pure MoS₂ monolayers. However, many reported as-grown monolayers frequently showed an XPS peak indicative of Mo⁶⁺ 3d_{3/2} from MoO₃ at ≈236.5 eV.^[4,18,19] Even though molybdenum oxides (MoO_x) are known to activate and transfer oxygen,^[20,21] are defective,^[22,23] and oxophilic,^[24] their effect on the oxidation of MoS₂ has not been systematically investigated.

Herein, we characterize the thermal oxidation of MoS₂ monolayers with and without MoO_x at atmospheric pressure in the temperature range of 25–400 °C using a novel ultrasensitive operando X-ray absorption spectroscopy (XAS). We report the first XAS measurement of an atomically thin monolayer MoS₂ under dynamic environments (i.e., temperature ramping up to 400 °C, 3 vol% O₂/He, 101.3 kPa, with X-rays in the energy range of 2–3 keV) and it is complemented by ex situ XAS, SEM, and XPS. Such unique measurements of monolayer species were performed using our newly designed operando XAS reactor that enables an ultrasensitive electron yield (EY) detection mode under actual reactive environments;^[25–29] different to conventional fluorescence and transmission modes (see Table S2, Supporting Information, for details). Our study shows that as-grown MoS₂ monolayers via CVD contain trace amounts of oxygenated Mo⁴⁺ and Mo⁶⁺. Without removing the MoO_x, the oxidation of MoS₂ monolayer was activated starting as low as 100 °C even in a diluted oxidative atmosphere at ambient pressure (3 vol% O₂ in inert gas). After removing MoO_x, the oxidation onset temperature of MoS₂ monolayers is increased to 300 °C. Our work shows that an oxide-free and high-purity monolayer MoS₂ is critical to the enhanced thermochemical stability of MoS₂.

To understand the effect of MoO_x on the MoS₂ oxidation, we prepared both as-grown (oxide-containing) and etched (oxide-free) MoS₂ monolayers with high quality supported on SiO₂/Si wafers (see Experimental Section, Supporting Text and Figures S1–S4, Supporting Information, for details). The etched monolayer MoS₂ was prepared by removing MoO_x via an alkaline-bath transfer treatment. We conducted electron microscopy, Raman, and XAS measurements to confirm that the etching step does not cause a structural and chemical change to the 2H-MoS₂ phase (Figures 1 and 2; Figures S1, S2, and S4, Supporting Information). Ex situ SEM images in Figure 1 show the morphological evolution of the as-grown and etched MoS₂ monolayers. For all SEM images, the light background indicates the SiO₂/Si support wafer (blue arrow), and the dark-colored triangular shapes are monolayer MoS₂ (red arrow) with tens of micrometers in size. Both the as-grown and etched MoS₂ samples appear to have unchanged global morphology even after oxidation at 350 °C, and both break up to small pieces at 400 °C (green arrow and dotted circles). The as-grown and some oxidized MoS₂ monolayers have lighter-color nanoparticles arranged in lines (Figure S5, Supporting Information) as marked by orange arrows and guided lines in Figure 1. The nanoparticles are ascribed to molybdenum oxides (MoO_x, vide infra). In comparison, those MoO_x nanoparticles are not seen on the etched MoS₂ (Figure 1k; Figure S6, Supporting Information), confirming the successful removal of oxide

species by the alkaline treatment, consistent with the Mo Pourbaix diagram.^[30] Finally, for the etched monolayer MoS₂, cracks and pits start to appear at 300 and 350 °C, which are indications of MoS₂ oxidation (Figure 1n,o; and high magnification images in Figure 1r,s) and are also observed in the as-grown MoS₂ at the same annealing temperatures (Figure 1d,e; and high magnification images in Figure 1h,i). Overall, the SEM results suggest that the oxidation onset temperature of MoS₂ monolayer is around 300 °C, regardless of the presence of MoO_x nanoparticles, which is consistent with previous oxidation studies.^[12–14]

The operando XAS characterization reveals the details of the oxidation behavior differences for MoS₂ monolayers with and without MoO_x, which are not captured by SEM images. Our new operando XAS reactor equipped with EY detection mode enables, for the first-time, XAS measurement of atomically thin MoS₂ monolayers under reactive conditions (see the experimental scheme of the reactor in Figure S7 and Table S2, Supporting Information). The X-ray beam spot size of 1 mm (vertical) × 3 mm (horizontal) is much larger than the single crystalline domain size of the monolayers (tens to around 100 μm). First, X-ray absorption near edge structure (XANES) spectra of reference standards were obtained in the EY mode under He atmosphere under ambient pressure at RT using commercial bulk MoS₂, MoO₂, and MoO₃ materials. The obtained spectra are consistent with the literature and our theoretical calculations (Figures S8 and S9, Supporting Information). Then, the S K-edge and Mo L_{3,2}-edge XANES spectra of the as-grown and etched MoS₂ monolayers were measured under He atmosphere at RT. Though their spectra are similar to the bulk MoS₂ material as shown in Figure 2, the as-grown MoS₂ monolayer shows additional shoulder peaks (black arrows) at 2528.6 eV in the Mo L₃-edge (Figure 2b) and 2633.5 eV in the Mo L₂-edge (Figure 2c), which indicates the presence of MoO_x.

After confirmation of the existence of MoO_x in the as-grown MoS₂ monolayers, operando XAS under the oxidative atmosphere was performed to follow the differences between the as-grown and etched MoS₂ monolayers with increasing temperature. The oxygen partial pressure used in the operando XAS electron yield reactor (3 vol% O₂/He, 101.3 kPa) was identical to that used for the ex situ XAS, SEM, and XPS studies. The MoS₂ monolayers were ramped to the desired temperature and held there for 30 min. Then, three consecutive overlapping XAS scans were recorded that show spectra reproducibility (Figure S10, Supporting Information), and the averaged spectra are used here. Figure 3 shows the operando XANES spectra of as-grown (Figure 3a,c) and etched (Figure 3b,d) MoS₂ monolayers under increasing temperatures (100–400 °C). The chemical evolutions of the as-grown and etched MoS₂ samples were monitored by following the S K-edge (Figure 3a,b) and Mo L₃-edge (Figure 3c,d) XANES spectra.

The evolution of the S K-edge spectra is similar for the MoS₂ monolayers with and without oxides. Both S K-edge spectra features of the as-grown and etched MoS₂ monolayers match with the bulk MoS₂ references for temperatures up to 350 °C, indicating that S atoms remain in the MoS₂ chemical composition (Figure 3a,b). At 400 °C, both S K-edge spectra show a new peak at 2482.6 eV, which is ascribed to S⁶⁺, likely in the form of sulfates.^[31] The difference in the intensity of the new S⁶⁺ peaks at 400 °C indicates that the as-grown sample oxidizes more than the etched monolayer MoS₂ (Figure 3a,b). The formation of

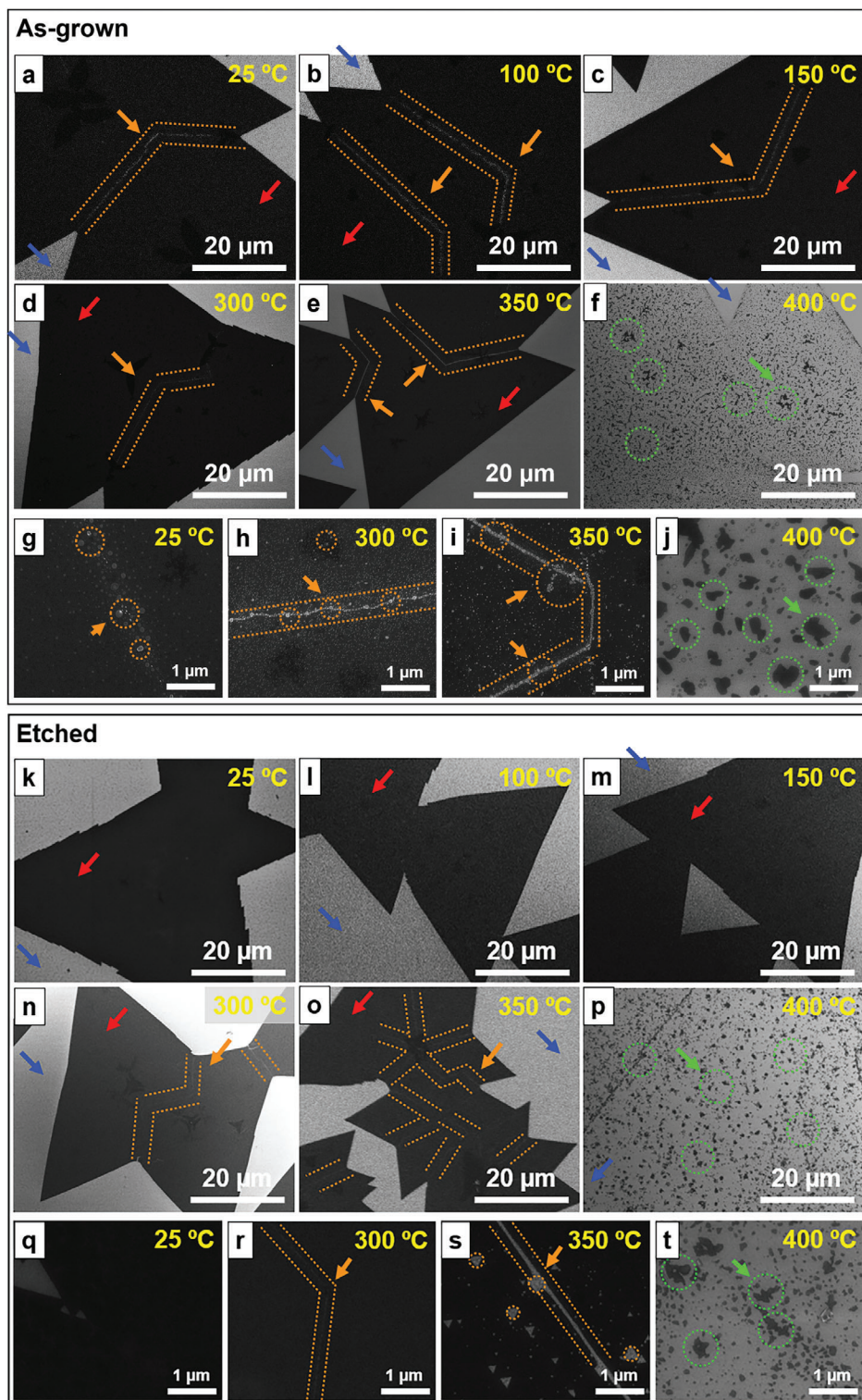


Figure 1. SEM images of the as-grown and etched MoS₂ monolayers before (25 °C) and after annealing (100–400 °C). a–j) The SEM images of the as-grown MoS₂ monolayers a,g) before annealing (25 °C) and after annealing at b) 100 °C, c) 150 °C, d,h) 300 °C, e,i) 350 °C, and f,j) 400 °C. k–t) The SEM images of the k,q) etched MoS₂ monolayers before annealing (25 °C) and after annealing at l) 100 °C, m) 150 °C, n,r) 300 °C, o,s) 350 °C, and p,t) 400 °C. The light background is the SiO₂/Si wafer (blue arrow) and monolayer MoS₂ appears as a dark flake (red arrow). The bright nanoparticles (enclosed by orange dotted lines and pointed by arrows) are ascribed as MoO_x nanoparticles. Both the f) as-grown and p) etched MoS₂ monolayers break into small pieces (green arrow and dotted circles) after being annealed at 400 °C. Ex situ SEM images were taken from different spots in different samples.

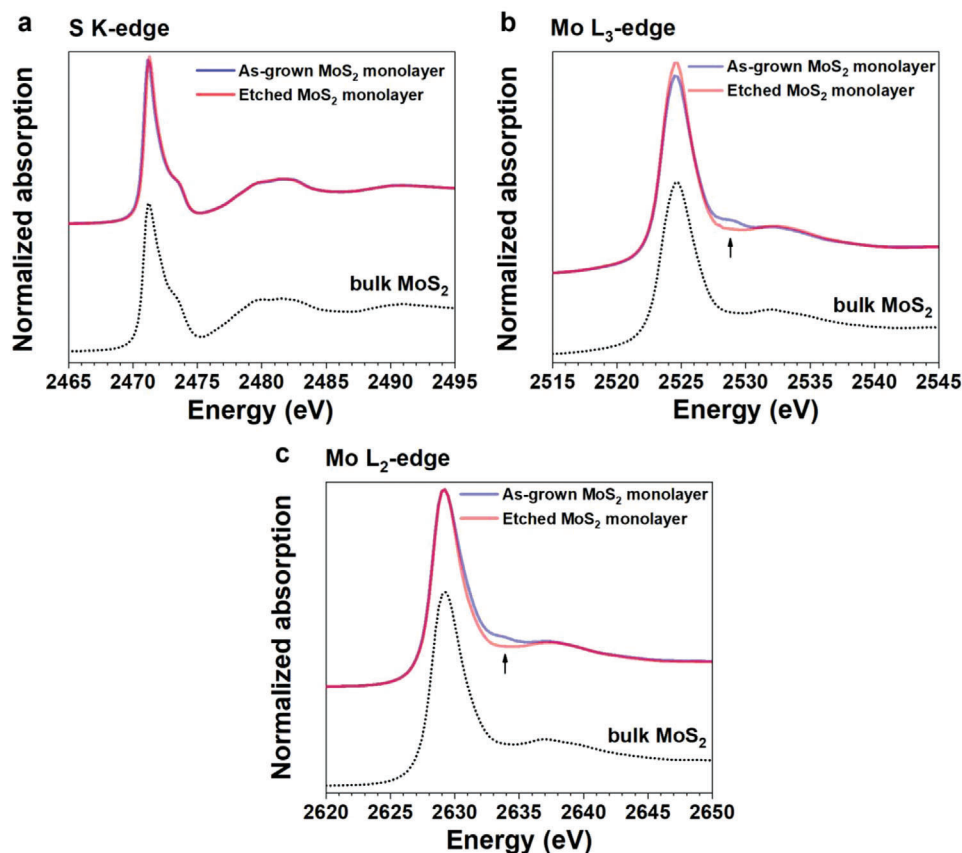


Figure 2. S K-edge and Mo $L_{2,3}$ -edges XANES spectra of the as-grown and etched MoS_2 monolayers with the bulk MoS_2 reference. a) The S K-edge, b) Mo L_3 -edge, and c) Mo L_2 -edge XANES spectra of the as-grown (blue) and etched (red) MoS_2 monolayers, and bulk MoS_2 standard reference (black dot) are measured at room temperature (RT) under He atmosphere before oxidation. b,c) The additional shoulder peaks on the Mo L_3 and L_2 -edge spectra at b) 2528.6 eV and c) 2633.5 eV, respectively, (black arrows) from the as-grown monolayer MoS_2 indicate that the as-grown monolayer MoS_2 contains MoO_x . The MoO_x can be successfully removed from MoS_2 monolayers by the alkaline bath treatment, which is confirmed through the removal of the additional shoulder peaks.

sulfates at 400 °C coincides with the severe morphological changes observed via SEM images (Figure 1f,p).

On the other hand, the operando Mo $L_{3,2}$ -edge XANES spectra show different evolution features between the as-grown and etched MoS_2 monolayers (Figure 3c,d). Those spectra were further subtracted by the spectra of the etched monolayer at 25 °C (i.e., pristine MoS_2 without oxides) to obtain the difference spectra (Figures 3e,f), which highlight the changes of spectra feature. For the as-grown MoS_2 monolayer, the first negative broad feature at 2524.5 eV ascribed to a combination of Mo^{4+} and Mo^{6+} grows with increasing temperature up to 300 °C. Then, the negative feature shifts 0.3 eV to lower energy, resembling Mo^{6+} as in the MoO_3 reference (Figure 3e). Likewise, the Mo L_3 -edge spectra show a gradually increased Mo^{6+} peak at 2528.6 eV with increasing temperature (Figure 3c,e). Finally, the Mo L_3 -edge white line is shifted from resembling MoS_2 to MoO_3 at 400 °C (Figure 3c,e). In comparison, for the etched sample, the Mo^{4+} and Mo^{6+} peaks ascribed to MoO_2 and MoO_3 become slightly apparent only at 300 °C, and the Mo L_3 -edge white line is shifted from resembling MoS_2 to MoO_3 at 400 °C (Figure 3d,f). The Mo L_2 -edge spectra show the same trends (Figure S11, Supporting Information). We cross-checked the operando XAS results by con-

ducting ex situ XAS of those MoS_2 monolayers shown in Figure 1, and the results are consistent (Figure S12, Supporting Information). First-principles simulations of XAS spectra with the OCEAN code^[32,33] show that O-substitution on S-vacancies in MoS_2 monolayers produces a sequential shift of the absorption edge with increasing oxygenation as observed in our experimental spectra (Figure 3c,e; Figure S13, Supporting Information). To summarize the Mo L_3 -edge operando XANES results, oxygenated Mo^{4+} and Mo^{6+} species are formed starting at 100 °C in the as-grown MoS_2 monolayer sample, and those species increase with increasing temperature (likely in the form of MoO_2 and MoO_3). In contrast, features ascribed to oxides start to appear at 300 °C for the etched MoS_2 monolayer sample. Furthermore, the as-grown MoS_2 monolayers are nearly completely oxidized at 400 °C, at which point, Mo^{6+} species (as in MoO_3) dominate the spectra; however, the etched MoS_2 monolayers still show a transition towards MoO_3 formation at 400 °C likely resulting in the spectral combination of MoO_2 and MoO_3 signals.

To quantitatively investigate the trend of chemical composition changes of the as-grown and etched MoS_2 monolayers at different temperatures, the linear combination fitting analysis (LCFA) of the operando Mo L_3 -edge XANES from Figure 3c,d

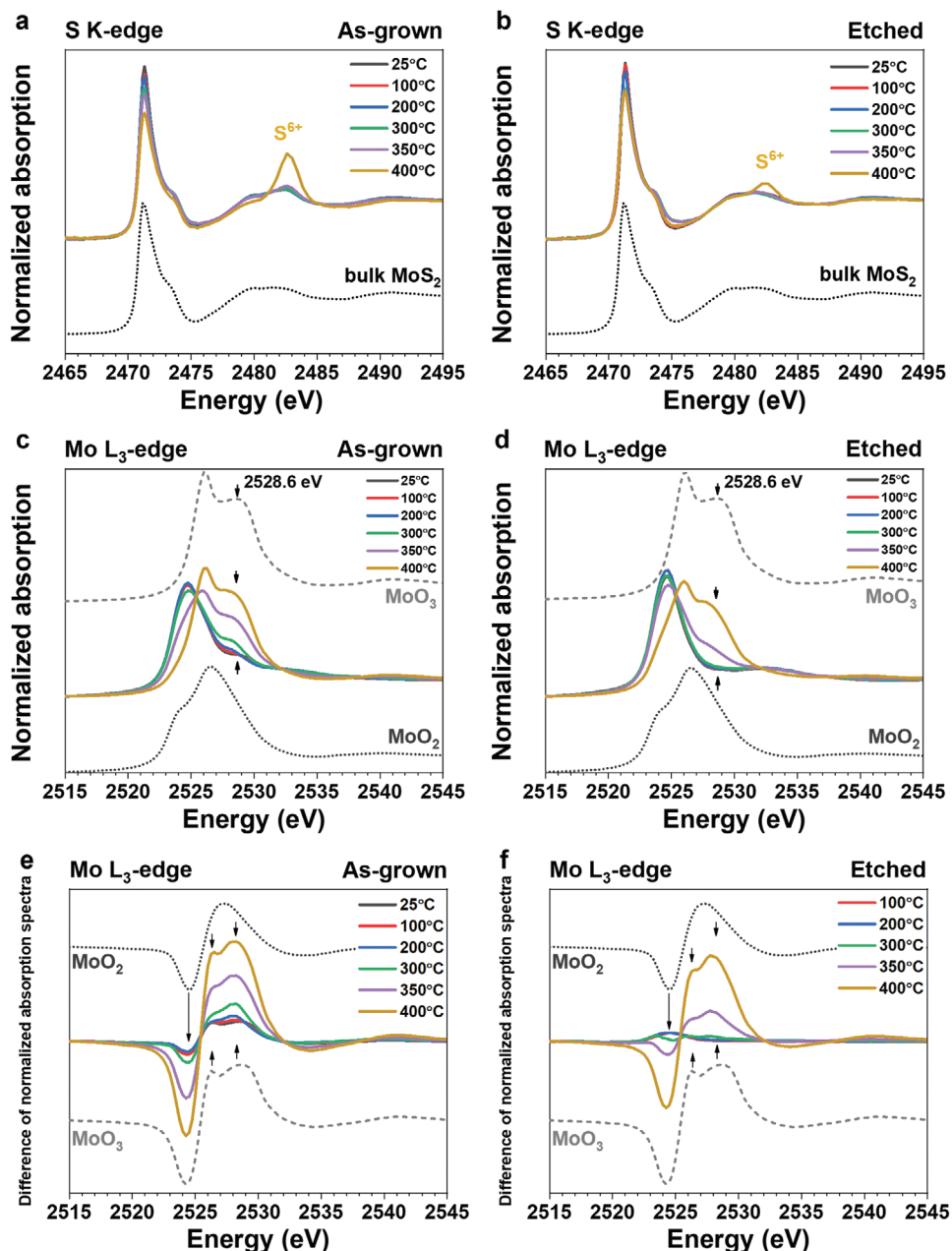


Figure 3. The operando S K-edge and Mo L₃-edge XANES spectra of the as-grown and etched MoS₂ monolayers under dilute oxidative atmosphere (3 vol% O₂/He) with increasing temperature (100–400 °C). a,b) The operando S K-edge XANES spectra of the a) as-grown and b) etched MoS₂ monolayers are shown. The spectra of the commercial bulk MoS₂ are included as references. The peak of S⁶⁺ is denoted at 2482.6 eV. c,d) The operando Mo L₃-edge XANES spectra of the c) as-grown and d) etched MoS₂ monolayers are shown. The prominent peak at 2528.6 eV generated by the gradual formation of MoO₃ is marked with black arrows. The spectra of the commercial MoO₂ and MoO₃ are included as references. e,f) The difference spectra of the Mo L₃-edge XANES spectra of the e) as-grown and f) etched MoS₂ monolayers are shown. The spectra of the commercial MoO₂ and MoO₃ are included as references. g,h) The chemical compositions of g) as-grown and h) etched MoS₂ monolayers after oxidation at different temperatures are estimated from linear combination fitting analysis (LCFA).

was performed,^[34] and the results are presented in Figure 3g,h (see Tables S3 and S4, Supporting Information, for details). First, the chemical analysis supports the existence of MoO_x in the as-grown MoS₂ monolayer, and on the contrary, the etched sample is composed of pure MoS₂. Second, the amount of MoO_x in the as-grown sample is found to gradually increase with in-

creasing temperature even at the low temperature of 100 °C, indicating the oxidation onset temperature (1% ± 1% MoO₂ and 3% ± 1% MoO₃ increase, and 5% ± 1% MoS₂ decrease). Third, the oxidation of the etched MoS₂ monolayer starts at 300 °C. Complementarily, the normalized sulfur concentration acquired from the S K-edge step as a function of temperature is shown in

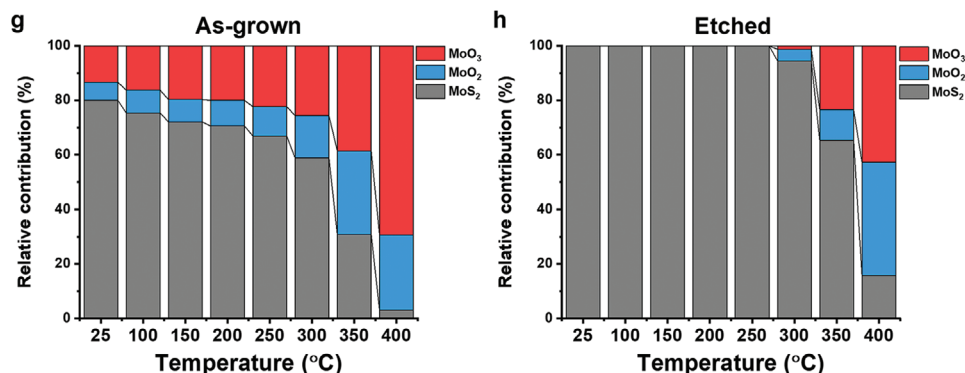


Figure 3. Continued

Figure S14, Supporting Information. The analysis of the edge step in the S K-edge XANES spectra shows that both the as-grown and etched MoS₂ monolayers start losing significant amounts of S at around 350 °C, indicating that rapid oxidation happens. Both as-grown and etched MoS₂ monolayers undergo severe chemical transformations at 400 °C. The as-grown monolayer MoS₂ loses on average $\approx 23\%$ more sulfur than the etched MoS₂ monolayer under the same high temperatures and oxidation conditions at 350 and 400 °C. Overall, the differences between the samples in XANES and the chemical analysis suggest that the presence of MoO_x lowers the onset temperature for fast thermal oxidation, promotes the oxidation reaction under the same temperature, and facilitates the sulfur loss in monolayer MoS₂. Building upon published literature on the catalytic properties of oxides of molybdenum,^[20,21] we propose that MoO_x facilitates O₂ dissociation ultimately lowering the onset oxidation temperature of as-grown MoS₂ monolayers down to 100 °C.

We further conducted complementary ex situ XPS at the O 1s, Mo 3d, and S 2p regions to confirm the impact of MoO_x on the oxidation process of MoS₂ monolayers. Figure 4a,d shows the O 1s spectra of the as-grown and etched MoS₂ monolayers that are fitted with two singlets, respectively. The main peak at 533.4 eV for both samples is assigned to Si–O from the SiO₂/Si substrate.^[35] The small peak at 531.4 eV corresponds to lattice Mo–O in oxide structures.^[12,36,37] For the as-grown MoS₂ monolayer, the O 1s peak intensity of Mo–O gradually increases from RT to 400 °C, so does the Mo⁶⁺ peaks at 236.5 eV (3d_{3/2}) and 233.5 eV (3d_{5/2}) in the Mo 3d region (Figure 4b).^[12,38,39] For the etched-MoS₂ layers, both the O 1s peak for Mo–O and the Mo⁶⁺ peaks are negligible below 300 °C (Figure 4d,e). The S 2p spectra show no significant differences throughout the oxidation process until 400 °C for both as-grown and etched samples (Figure 4c,f). For both as-grown and etched samples, the MoS₂ monolayers seem to be nearly fully oxidized at 400 °C (Mo⁶⁺ $\approx 90\%$, Figure S15, Supporting Information), as evidenced by the weak intensity of S 2p (Figure S16, Supporting Information; ten times magnified counts than in Figure 4f) and 2s peaks, and Mo⁴⁺ peaks at 233.3 eV (3d_{3/2}) and 230.2 eV (3d_{5/2}) in the Mo 3d region.^[12,38,39] The XPS results support the observations from the operando XANES spectra (Figure 3) in that MoO_x activates the oxidation of MoS₂ monolayer from the low temperature at 100 °C. Nevertheless, operando XANES shows advantages by providing quantitative and qualitative information of chemical changes with better sensitivity, such

as the sulfur loss and chemical specificity with increasing temperature under reactive and dynamic environmental conditions. Ultimately, operando XAS provides the accurate chemical composition evolution of the reaction products under the actual working conditions of 2D devices.

In summary, we reveal for the first time the low-temperature thermal oxidation of monolayer MoS₂ promoted by MoO_x. Our pioneering ultrasensitive operando XAS study shows that the as-grown MoS₂ monolayers (via CVD) contain MoO₂ and MoO₃ impurities (i.e., MoO_x) and that the amount of the oxides increases with increasing MoS₂ oxidation even with exposures to diluted O₂ at the low temperature of 100 °C (3 vol% O₂/He, 101.3 kPa). In comparison, the etched MoS₂ monolayers remain pristine until heating to 300 °C. The difference indicates that MoO_x promotes the oxidation of MoS₂ monolayers under the operation conditions of 2D devices. The available S atoms remain in a similar chemical and structural environment up to 350 °C, at which point MoS₂ oxidizes to MoO₃ and other volatile species. These results are supported by systematic ex situ XAS, XPS, and SEM characterizations. The results demonstrate that the oxide-free condition is critical to the long-term thermochemical stability of monolayer MoS₂, which is expected to hold for other transition metal dichalcogenides monolayers with crucial implications for emerging scalable 2D electronic, optical, and catalytic applications.

Supporting Information

Supporting Information is available from the Wiley Online Library or from the author.

Acknowledgements

S.P. and A.T.G.-E. contributed equally to this work. The authors acknowledge the financial support of the Stanford Precourt Institute for Energy and Stanford Natural Gas Initiative. S.P. acknowledges the generous financial support from the Kwanjeong Educational Foundation. Use of the Stanford Synchrotron Radiation Lightsources, SLAC National Accelerator Laboratory, was supported by the U.S. Department of Energy, Office of Science, Office of Basic Energy Sciences under contract no. DE-AC02-76SF00515. Part of this work was performed at the Stanford Nano Shared Facilities (SNSF)/Stanford Nanofabrication Facility (SNF), supported by the National Science Foundation under award ECCS-1542152. This research used resources of the National Energy Research Scientific Computing Center

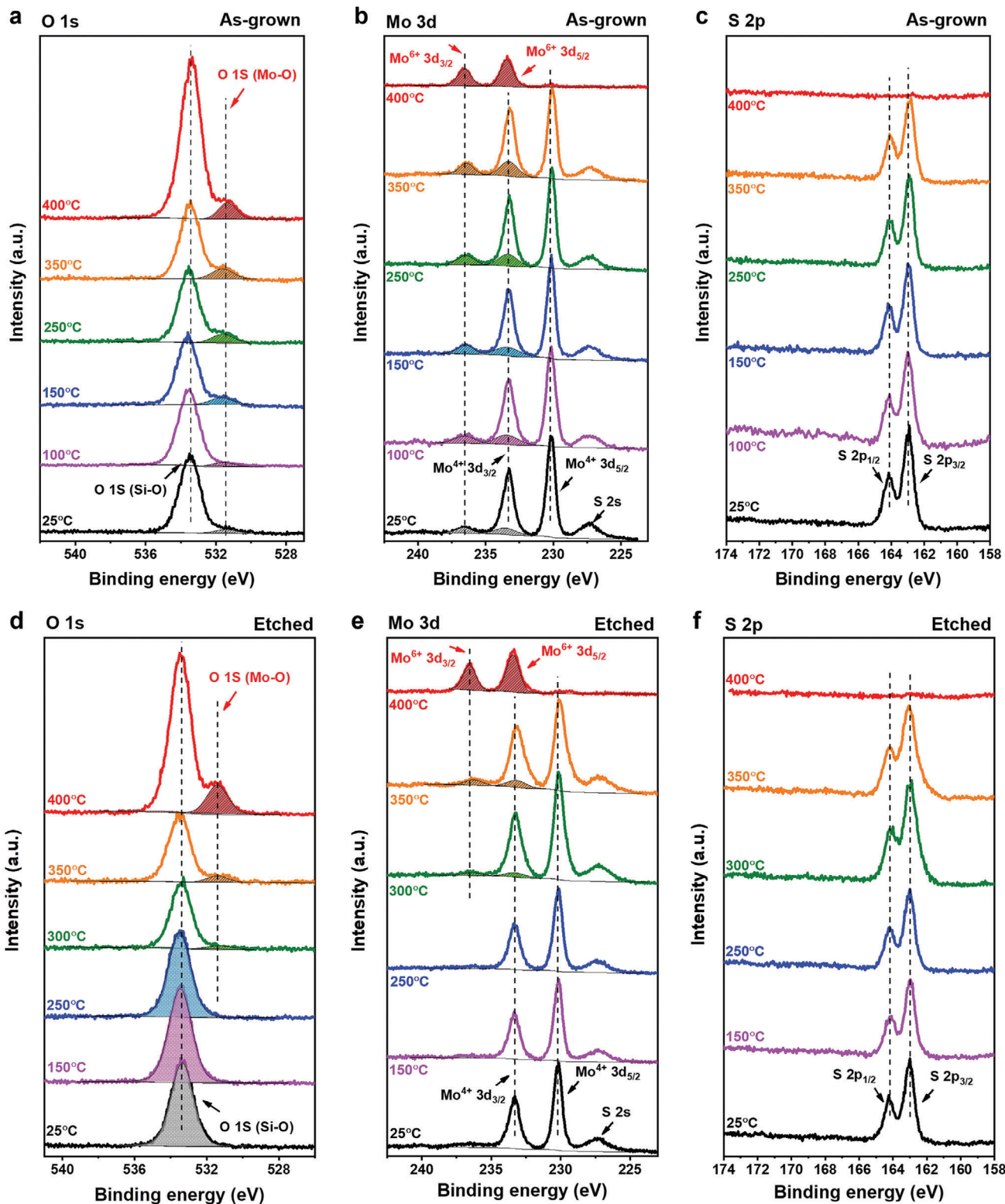


Figure 4. XPS spectra of O 1s, Mo 3d, and S 2p regions of the as-grown and etched MoS₂ monolayers before (25 °C) and after annealing (100–400 °C). a,d) XPS spectra of O 1s region of the a) as-grown and d) etched MoS₂ monolayers. The O 1s spectra are noted and partially fitted with the Mo–O (filled color with lines) and Si–O (filled color with dots) peaks. b,e) XPS spectra of Mo 3d region of the b) as-grown and e) etched MoS₂ monolayers. The Mo 3d spectra are noted and partially fitted with Mo⁶⁺ 3d_{3/2} and 3d_{5/2} peaks (filled color with lines). The other prominent peaks such as Mo⁴⁺ 3d_{3/2} and 3d_{5/2}, and S 2s are denoted in each peak energy position. c,f) XPS spectra of the S 2p region of the c) as-grown and f) etched MoS₂ monolayers. The prominent peaks of S 2p_{1/2} and 2p_{3/2} are denoted in each peak energy position.

(NERSC), a U.S. Department of Energy Office of Science User Facility operated under contract no. DE-AC02-05CH11231. A.G. thanks the support by the U.S. Department of Energy, Office of Science, Office of Basic Energy Sciences, Chemical Sciences, Geosciences, and Biosciences Division, Catalysis Science Program to the SUNCAT Center for Interface Science and Catalysis.

Conflict of Interest

The authors declare no conflict of interest.

Data Availability Statement

Research data are not shared.

Keywords

2D materials, monolayer molybdenum disulfide, operando oxidation, thermochemistry

Received: July 22, 2020

Revised: January 12, 2021

Published online: March 1, 2021

- [1] B. Radisavljevic, A. Radenovic, J. Brivio, V. Giacometti, A. Kis, *Nat. Nanotechnol.* **2011**, *6*, 147.
- [2] J. Lee, S. Pak, P. Giraud, Y. W. Lee, Y. Cho, J. Hong, A. R. Jang, H. S. Chung, W. K. Hong, H. Y. Jeong, H. S. Shin, L. G. Occhipinti, S. M. Morris, S. Cha, J. I. Sohn, J. M. Kim, *Adv. Mater.* **2017**, *29*, 1702206.
- [3] H. M. Hill, A. F. Rigosi, K. T. Rim, G. W. Flynn, T. F. Heinz, *Nano Lett.* **2016**, *16*, 4831.
- [4] V. K. Sangwan, H. S. Lee, H. Bergeron, I. Balla, M. E. Beck, K. S. Chen, M. C. Hersam, *Nature* **2018**, *554*, 500.
- [5] D. Akinwande, N. Petrone, J. Hone, *Nat. Commun.* **2014**, *5*, 5678.
- [6] M. Park, Y. J. Park, X. Chen, Y. K. Park, M. S. Kim, J. H. Ahn, *Adv. Mater.* **2016**, *28*, 2556.
- [7] K. Kang, S. Xie, L. Huang, Y. Han, P. Y. Huang, K. F. Mak, C. J. Kim, D. Muller, J. Park, *Nature* **2015**, *520*, 656.
- [8] J. Shim, S.-H. Bae, W. Kong, D. Lee, K. Qiao, D. Nezich, Y. J. Park, R. Zhao, S. Sundaram, X. Li, H. Yeon, C. Choi, H. Kum, R. Yue, G. Zhou, Y. Ou, K. Lee, J. Moodera, X. Zhao, J.-H. Ahn, C. Hinkle, A. Ougazzaden, J. Kim, *Science* **2018**, *362*, 665.
- [9] K. Kang, K. H. Lee, Y. Han, H. Gao, S. Xie, D. A. Muller, J. Park, *Nature* **2017**, *550*, 229.
- [10] E. Yalon, C. J. McClellan, K. K. H. Smithe, M. Munoz Rojo, R. L. Xu, S. V. Suryavanshi, A. J. Gabourie, C. M. Neumann, F. Xiong, A. B. Farimani, E. Pop, *Nano Lett.* **2017**, *17*, 3429.
- [11] K. F. Mak, K. L. McGill, J. Park, P. L. McEuen, *Science* **2014**, *344*, 1489.
- [12] D. M. Sim, M. Kim, S. Yim, M.-J. Choi, J. Choi, S. Yoo, Y. S. Jung, *ACS Nano* **2015**, *9*, 12115.
- [13] W. L. Spychalski, M. Pisarek, R. Szożkiewicz, *J. Phys. Chem. C* **2017**, *121*, 26027.
- [14] M. Yamamoto, T. L. Einstein, M. S. Fuhrer, W. G. Cullen, *J. Phys. Chem. C* **2013**, *117*, 25643.
- [15] T. H. Ly, M.-H. Chiu, M.-Y. Li, J. Zhao, D. J. Perello, M. O. Cichocka, H. M. Oh, S. H. Chae, H. Y. Jeong, F. Yao, L.-J. Li, Y. H. Lee, *ACS Nano* **2014**, *8*, 11401.
- [16] R. Szożkiewicz, M. Rogala, P. Dabrowski, *Materials* **2020**, *13*, 3067.
- [17] S. Park, S. Siahrostami, J. Park, A. H. B. Mostaghimi, T. R. Kim, L. Vallez, T. M. Gill, W. Park, K. E. Goodson, R. Sinclair, X. Zheng, *Adv. Mater.* **2020**, *32*, 2003020.
- [18] X. Zhang, J. Grajal, J. L. Vazquez-Roy, U. Radhakrishna, X. Wang, W. Chern, L. Zhou, Y. Lin, P. C. Shen, X. Ji, X. Ling, A. Zubair, Y. Zhang, H. Wang, M. Dubey, J. Kong, M. Dresselhaus, T. Palacios, *Nature* **2019**, *566*, 368.
- [19] S. Bettis Horman, V. K. Sangwan, I. Balla, H. Bergeron, E. A. Weiss, M. C. Hersam, *Nano Lett.* **2017**, *17*, 164.
- [20] R. H. Holm, *Chem. Rev.* **1987**, *87*, 1401.
- [21] H. Arzoumanian, *Coord. Chem. Rev.* **1998**, *178–180*, 191.
- [22] N. Zhang, X. Li, H. Ye, S. Chen, H. Ju, D. Liu, Y. Lin, W. Ye, C. Wang, Q. Xu, J. Zhu, L. Song, J. Jiang, Y. Xiong, *J. Am. Chem. Soc.* **2016**, *138*, 8928.
- [23] A. Ruiz Puigdollers, P. Schlexer, S. Tosoni, G. Pacchioni, *ACS Catal.* **2017**, *7*, 6493.
- [24] K. P. Kepp, *Inorg. Chem.* **2016**, *55*, 9461.
- [25] A. Erbil, I. G. Cargill, R. Frahm, R. F. Boehme, *Phys. Rev. B: Condens. Matter Mater. Phys.* **1988**, *37*, 2450.
- [26] W. T. Elam, J. P. Kirkland, R. A. Neiser, P. D. Wolf, *Phys. Rev. B: Condens. Matter Mater. Phys.* **1988**, *38*, 26.
- [27] G. D. Moggridge, T. Rayment, R. M. Ormerod, M. A. Morris, R. M. Lambert, *Nature* **1992**, *358*, 658.
- [28] R. B. Greegor, N. E. Pingitore Jr., F. W. Lytle, *Science* **1997**, *275*, 1452.
- [29] J.-J. Velasco-Velez, C. H. Wu, T. A. Pascal, L. F. Wan, J. Guo, D. Prendergast, M. Salmeron, *Science* **2014**, *346*, 831.
- [30] A. G. Tyurin, *Prot. Met.* **2003**, *39*, 367.
- [31] E. D. Risberg, F. Jalilehvand, B. O. Leung, L. G. Pettersson, M. Sandstrom, *Dalton Trans.* **2009**, 3542.
- [32] J. Vinson, J. J. Rehr, J. J. Kas, E. L. Shirley, *Phys. Rev. B: Condens. Matter Mater. Phys.* **2011**, *83*, 115106.
- [33] K. Gilmore, J. Vinson, E. L. Shirley, D. Prendergast, C. D. Pemmaraju, J. J. Kas, F. D. Vila, J. J. Rehr, *Comput. Phys. Commun.* **2015**, *197*, 109.
- [34] E. S. Jeong, C. I. Park, Z. Jin, I. H. Hwang, J. K. Son, M.-Y. Kim, J.-S. Choi, S.-W. Han, *Catal. Lett.* **2015**, *145*, 971.
- [35] H. A. Duarte, M. E. Sad, C. R. Apesteeguía, *Catal. Today* **2019**, *356*, 399.
- [36] J. Liu, S. Tang, Y. Lu, G. Cai, S. Liang, W. Wang, X. Chen, *Energy Environ. Sci.* **2013**, *6*, 2691.
- [37] D. Guan, J. Li, X. Gao, C. Yuan, *J. Power Sources* **2014**, *246*, 305.
- [38] J. Kibsgaard, Z. Chen, B. N. Reinecke, T. F. Jaramillo, *Nat. Mater.* **2012**, *11*, 963.
- [39] J. Gao, B. Li, J. Tan, P. Chow, T. M. Lu, N. Koratkar, *ACS Nano* **2016**, *10*, 2628.